

Article

Assessment of the Tribological Properties of Aluminum Matrix Composites Intended for Cooperation with Piston Rings in Combustion Engines

Anna Janina Dolata ^{1,*}, Jakub Wieczorek ¹, Maciej Dyzia ¹ and Michał Starczewski ²

¹ Faculty of Materials Engineering, Silesian University of Technology, Krasińskiego 8 St., 40-019 Katowice, Poland; jakub.wieczorek@polsl.pl (J.W.); maciej.dyzia@polsl.pl (M.D.)

² ZŁOTECKI Ltd., Żelechlin 2 St., 88-110 Rojewo, Poland; michal.starczewski@zlolecki.pl

* Correspondence: anna.dolata@polsl.pl; Tel.: +48-(32)-603-4426

Abstract: Tribological interactions between the piston groove and ring in combustion engines have a significant influence on mechanical friction losses. Based on the analysis of the distribution of forces acting on the piston, the conditions for the friction tests were selected. The research was carried out on composites reinforced with silicon carbide (SiC_p), glassy carbon (GC_p), and a hybrid mixture of particles (SiC_p + GC_p). Tribological tests were carried out under extremely unfavorable dry sliding conditions using a pin-on-block tester. The friction coefficient and wear values of the matrix alloy, composites, and iron were compared. Profilometry was used to perform quantitative and qualitative analyses of the wear tracks formed on the tested surfaces. The effect of the presence of reinforcing particles on the geometry of working surfaces was also evaluated. The obtained results show that AlSi12CuNiMg/SiC_p and AlSi12CuNiMg/SiC_p + GC_p composites provided satisfactory effects towards stabilizing the friction coefficient and reducing the wear of tested tribological couples. This may provide a new solution dedicated to an important system, which is the piston groove/piston ring in diesel engines.

Keywords: aluminum matrix composites (AIMCs); ceramic reinforcement; silicon carbide; glassy carbon; tribological properties; piston; piston rings



Citation: Dolata, A.J.; Wieczorek, J.; Dyzia, M.; Starczewski, M. Assessment of the Tribological Properties of Aluminum Matrix Composites Intended for Cooperation with Piston Rings in Combustion Engines. *Materials* **2022**, *15*, 3806. <https://doi.org/10.3390/ma15113806>

Academic Editor:
Nektaria-Marianthi Barkoula

Received: 16 April 2022

Accepted: 24 May 2022

Published: 26 May 2022

Publisher's Note: MDPI stays neutral with regard to jurisdictional claims in published maps and institutional affiliations.



Copyright: © 2022 by the authors. Licensee MDPI, Basel, Switzerland. This article is an open access article distributed under the terms and conditions of the Creative Commons Attribution (CC BY) license (<https://creativecommons.org/licenses/by/4.0/>).

1. Introduction

In the automotive industry and in certain areas of the heavy machine industry, road machinery, power generators, agricultural machinery, and piston engines are still the main power sources. This has caused a constantly growing interest in new construction solutions to increase the efficiency of combustion engines with different purposes. Innovative work is being conducted in a few different related areas. There is a search for effective and efficient new ways of lubrication and effective methods for using the heat generated during engine operation [1]. Increasing the strength and reliability of both the engine and its main components, while reducing fuel consumption and toxic emissions of exhaust gases, is also being pursued [2,3]. Therefore, innovative work is carried out in many different areas, from control automation and new construction solutions to materials engineering. In the field of materials engineering, the main role is played by research and the implementation of metal matrix composites (MMCs). Particularly, composites based on lightweight aluminum alloys (AIMCs) reinforced with hard ceramic particles, mainly oxides (i.e., Al₂O₃, SiO₂, and TiO₂) or carbides (SiC, TiC, and TiC) show great potential [4–10]. Due to their unique properties and the ability to tune these properties, AIMCs constitute an interesting group of materials dedicated to the construction of innovative internal combustion engines, as well as gas compressors and reciprocating pumps [11–13].

In practice, aluminum piston suppliers use a wide range of optimized alloy compositions that are generally based on silumins (such as Al-7% Si hypoeutectic, Al-12% Si eutectic,

and hypereutectic alloys with 18 and 24% Si) [14–17]. Particle-reinforced aluminum matrix composites (PAIMCs), mainly those with silicon carbide (SiC_p), are very promising and may provide an alternative to the currently used un-reinforced Al–Si alloys [18–22]. Compared to matrix alloys, AlSi/SiC_p composites are characterized by a higher strength and rigidity—especially at elevated temperatures—more stable thermal coefficients of expansion, and increased hardness and resistance to abrasive wear [23–26]. Based on the tribological and thermal properties of such composite materials, the author’s works [13,27,28] have focused on the concept of using this kind of material in the piston-rings-cylinder liner (PRC) assembly.

Forces Acting on the Piston Compression Rings

To ensure the proper application of materials, including composite materials, it is essential for understanding the force distribution on the construction element. During operation, a combustion engine piston is under a complex system of stresses, which has been widely discussed, analyzed, and described by many authors [29–34].

It should be noted that the main function of piston rings is to seal the combustion chamber against the crankcase. In turn, inter-ring dynamics are highly affected by inter-ring fluid dynamics, and many authors have considered both phenomena together, similar to Selmani et al. [34]. The forces acting on the piston rings were discussed by Niewczas et al. [29]. The authors presented several models that took into account the twists of the rings, the presence of an oil film, and the surface roughness and surface wear of the ring and groove. Similar models were shown by Wolff et al. [30–32]. The authors developed a complex model for the piston ring operation, taking into account a model of the gas flow through the labyrinth seal piston-rings-cylinder and a model of the oil flow in the lubrication gap between the ring and cylinder liner [32]. They pointed out that at high temperatures the oil viscosity is very low and consequently the oil film thickness is very thin along the cylinder liner. In this case, it is important to consider the mixed lubrication model and surface roughness of materials. The effect of the top ring geometry profile on the tribological characteristics of a low-displacement diesel engine was analyzed by Furero et al. [33]. The authors observed that the geometric profile of the compression ring modified the friction force caused by surface roughness. The scheme of the forces acting on the compression piston ring, prepared based on ref. [29], is shown in Figure 1. The most general form of the ring sliding surface profile and the partial oil filling of the gap between the ring and cylinder was assumed, similarly to refs. [29–32,34].

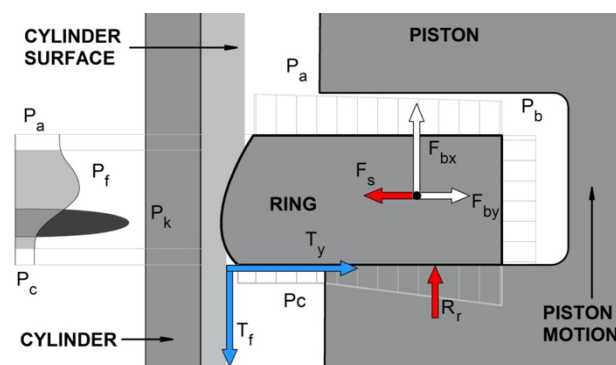


Figure 1. Forces acting on the first piston compression ring, where P_a , P_b , P_c —pressure in volumes above, behind, and below the ring, respectively; F_{bx} , F_{by} —ring inertia forces, acting in the axial and radial directions; F_s —ring elastic force; T_f , T_y —ring friction forces acting on the cylinder liner surface and piston groove shelf, respectively; P_f , P_k —oil film pressure and contact pressure with surface irregularities, respectively; and R_r —reaction force of the piston shelf, based on ref. [29].

The main forces acting on the piston compression ring (Figure 1) in the axial direction can be characterized as follows:

- P_a —the pressure acting on the upper-surface ring. In the case of the top compression ring, it is often assumed to be the pressure inside the combustion chamber;
- P_c —the pressure from the inter-ring space (below the ring) acting on the lower surface of the ring (the surface protruding beyond the piston groove). In this case, the force is directed upwards and tries to lift the ring from the lower shelf of the piston groove;
- T_f —the friction force acting on the working surface of the ring in contact with the cylinder (always acts opposite to the piston motion). It lifts and pushes the ring towards the lower shelf of the piston groove. This force is affected by the ring elastic force (F_s), the pressure of the ring gases on the cylinder surface, and the quality of lubrication;
- F_{bx} —the axial component of the inertia force (always directed opposite to the acceleration direction of the piston). In the case of the upper position of the piston, this force tends to pull the ring away from the lower groove shelf. While, in the lower position, it presses the ring to the shelf;
- R_r —the reaction force of the lower piston shelf on the side surface of the ring, directed opposite to the force pressing the ring to the shelf.

In the radial direction (Figure 1), the piston ring is affected by the following forces:

- F_s —the force caused by the self-elasticity of the ring, which is dependent on the ring construction;
- P_a —the force created by the working agent pressure, acting radially on the ring. This is the main part of the pressing and sealing forces of the PRC assembly;
- T_y —the friction force between the side surface of the ring and the piston groove. It works during the radial movement of the ring and can be caused by piston torsion inside the cylinder when the movement direction changes or if the cylinder is deformed. This force, depending on the piston position, can lift or press down the ring against the cylinder surface (Figure 2).

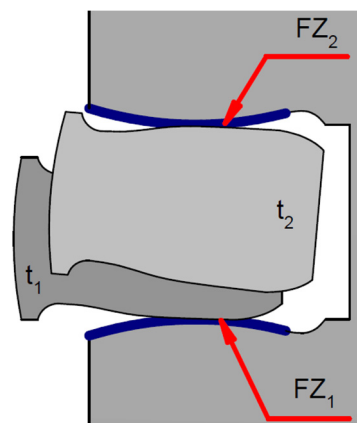


Figure 2. Wear of the piston ring and piston shelf as a result of their cooperating, where: t_1 —ring position relative to the piston groove shelf at time t_1 ; FZ_1 —friction zone (ring—lower shelf) at time t_1 ; t_2 —ring position relative to the piston shelf at time t_2 ; and FZ_2 —friction zone (ring—lower shelf) at time t_2 .

As a result of the cooperation of the piston ring with the surface of the piston groove, the shape of the geometric profile of these elements changes (Figure 2). The scale of the wear phenomenon near the piston groove and the piston ring was discussed by Niewczas et al. [29]. The authors estimated that after 300 h of engine operation (which is about 30,000 km during normal operation conditions), the value of the nominal piston ring clearance in the groove doubled.

Due to the above, to increase the wear resistance in highly loaded diesel engines, a cast iron insert is used for the first ring groove (Figure 3). The most important issue for such a solution is the strong connection between the ring carrier and piston material. Therefore, a

special Al-Fin casting process should be carried out to prepare the ferrous surface before casting non-ferrous Al alloy pistons [35,36].

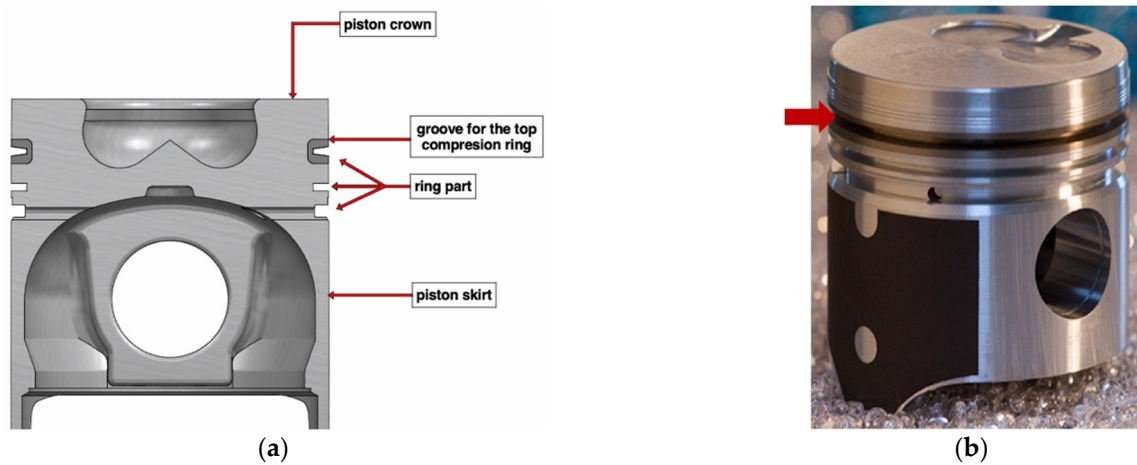


Figure 3. Piston for diesel engines with a cast iron insert: (a) Scheme of the piston cross-section divided into key components and (b) View of the piston; the arrow marks the area reinforced with a cast iron insert [37].

Our research focuses on the possibility of using AIMCs as an alternative to the materials that are currently used in the production of pistons, cylinder liners, and cast-iron inserts. Compared with previous works [13,27,28], the tribological properties of composite materials were assessed after cooperation with an iron sealing ring applied in the internal combustion engines (4CT90 produced by Andoria S.A., Andrychów, Poland).

2. Materials and Methods

2.1. Matrix, Reinforcement, and Composite Materials

The tested materials were PAIMCs based on the EN-AC 48000 aluminum alloy (AlSi12CuNiMg) reinforced with SiC_p, GC_p ceramic particles, and their hybrid powder mixture (SiC_p + GC_p). The microstructure of the un-modified AlSi12 matrix alloy and the morphology of reinforcing phases is shown in Figure 4.

To improve the wetting between metal and ceramic compounds [38], the chemical composition of the eutectic base AlSi12 alloy was modified by adding 1% Mg (Table 1). For this purpose, an AlMg25 master alloy produced by the Institute of Non-Ferrous Metals in Skawina was used. The composite suspension was obtained by a stir-casting method and formed into the sleeves using a centrifugal casting process. The technological procedures have been described in previously published papers [27,28,39–41]. The microstructure of AlSi12CuNiMg2/SiC_p 10 wt% composite is shown in Figure 5.

Table 1. Chemical composition ¹ of EN AC 48000 (AlSi12CuNiMg) commercial alloy * and modified by adding 1% Mg **.

Alloy Composition	Si	Mg	Cu	Ni	Fe	Mn	Ti	Al
AlSi12CuNiMg *	11.98	1.04	0.97	0.89	0.48	0.19	0.05	Bal.
AlSi12CuNiMg2 **	11.48	2.07	2.07	0.85	0.47	0.17	0.05	Bal.

¹ Alloy composition tested by mass spectrometry (Foundry Master, Oxford Instruments—WAS, Abingdon, UK).

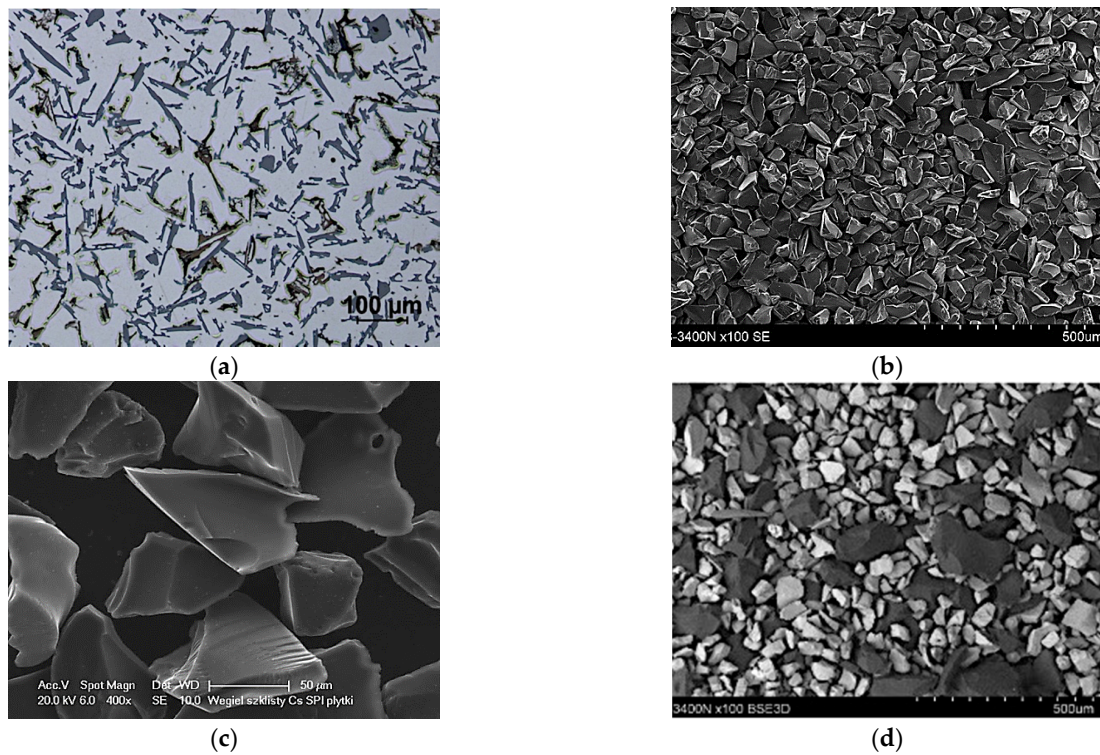


Figure 4. Microstructure of the base AlSi12 matrix alloy and the morphology of ceramic reinforcement: (a) AlSi12CuNiMg, LM; (b) silicon carbide (SiC_p), SEM; (c) glassy carbon (GC_p), SEM; and (d) SiC_p + GC_p hybrid powder mixture, SEM.

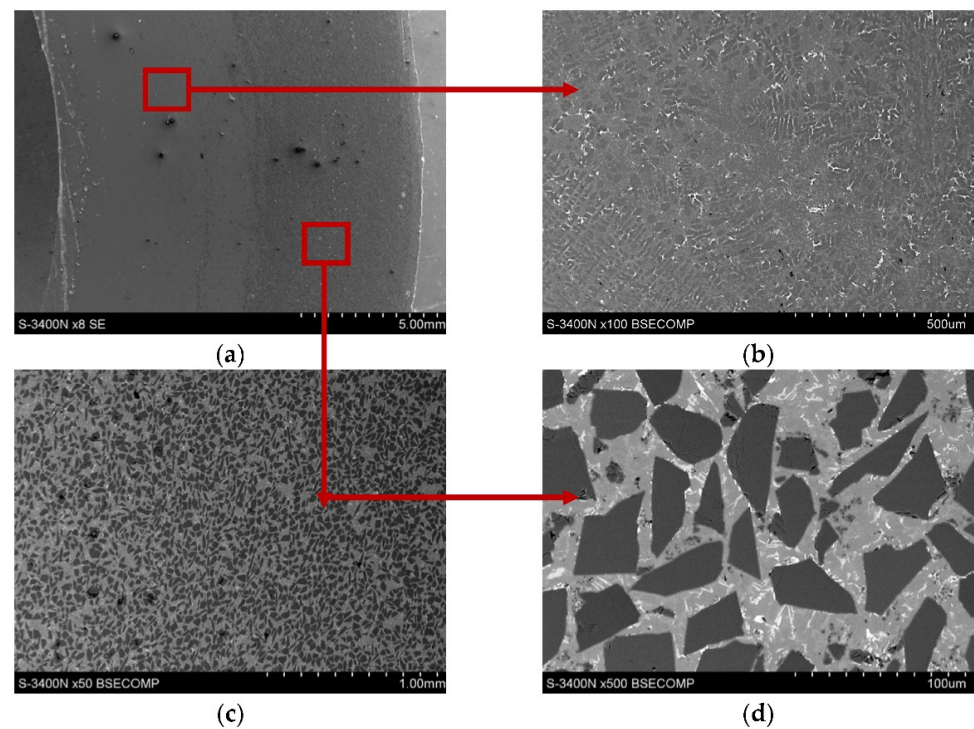


Figure 5. Cross-section perpendicular to the rotational axis of centrifugal cast obtained with AlSi12CuNiMg₂/SiC_p 10 wt% composite suspension; the red arrows indicates the microstructure of the Al/SiC_p composite layer: (a) macrostructure with visible outer composite layer, SEM; (b) microstructure of modified Al matrix alloy (area without SiC_p), SEM; and (c,d) microstructure of SiC_p particle-rich region, SEM.

2.2. Tribological Studies and Profilometry Analyses

The tests of the friction coefficient (COF) and wear of the materials were conducted at room temperature ($T = 20\text{ }^{\circ}\text{C}$) under technically dry friction conditions using a pin-on-block tribo-tester (Figure 6, Table 2). The scope of work was as follows:

- Preparation of samples through cutting the composite sleeves into discs $\sim 5\text{ mm}$ thick;
- Preparation of counter-pins by cutting out a fragment of the sealing ring and attaching it to the holder;
- Tribological tests on a block-pin tester in dry friction conditions;
- Measurement of the friction coefficient and profilometry analysis of the wear traces.

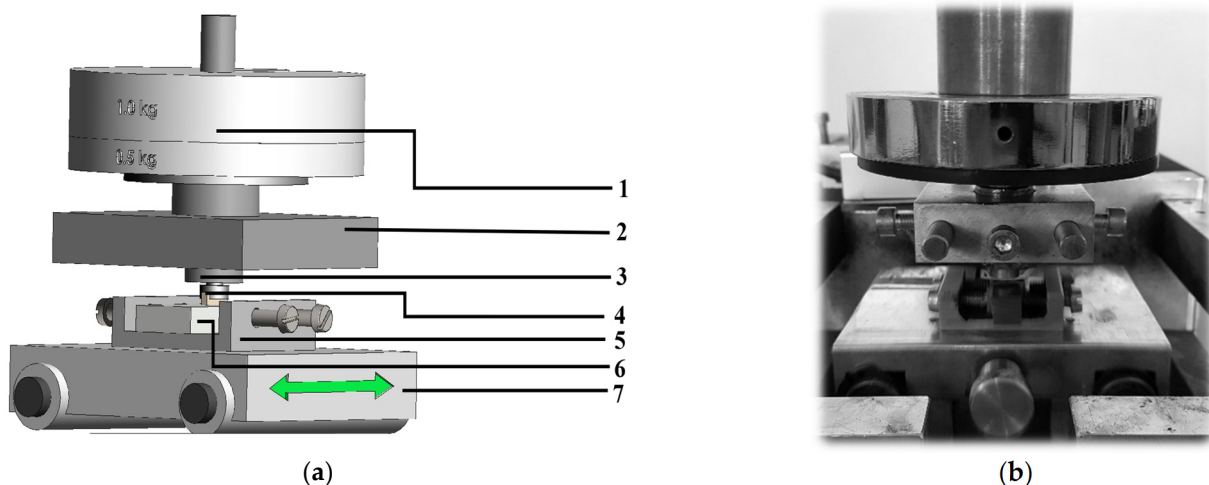


Figure 6. The experimental pin-on-block set-up used in tribological tests: (a) scheme of the stand, where: 1—Load, 2—strain gauge holder, 3—sample holder (pin), 4—cast iron pin, 5—sample holder (block), 6—composite sample, and 7—movable plate; and (b) view of the stand.

Table 2. The parameters used in tribological tests.

Sliding Speed [m/s]	Normal Load [N]	Distance [m]	Temperature [$^{\circ}\text{C}$]	Unit Pressure [MPa]
0.7	15	1200	20	0.8

During tribological tests, the friction load was measured continuously by using a strain gauge connected with an analog-digital converter and recorder. Using the registered values, the coefficient of friction (μ) was calculated as a function of sliding distance based on the author's software. The software is a dedicated statistical calculator that was designed to analyze a large number of measurement points (time and force) recorded during tribological tests. It averages sector data and presents them in the form of graphs of friction distance versus COF. The designation of the friction pairs used in tribological tests is presented in Table 3.

Table 3. Designation of samples and friction pairs used in tribological tests.

Material Designation	Reinforcing Particles	Volume of Particles [wt%]	Average Particle Diameter [μm]	Friction Counter Pin
AlSi12	-	-	-	GJL
AlSi12/SiC	SiC _p	10	58	GJL
AlSi12/GC	GC _p	10	80	GJL
AlSi12/SiC + GC	SiC _p + GC _p	7 + 3	58 and 80, respectively.	GJL
GJL	-	-	-	GJL

The analysis of the friction area of composites and cast-iron pins was conducted using profilometry measurements using a MicroProf 3000, FRT optical profilometer with an WCL3000 aberration head, (FRT GmbH, München, Germany) [28]. It is a non-contact measurement, so it completely eliminates the possibility of deforming the friction trace during the test. A study of the wear trace geometry was conducted immediately after the friction process. Only an ethanol solution was used to clean the surface of the tested samples. The surface geometry was evaluated using the following parameters: measurement area of $8 \times 8 \text{ mm}^2$; resolution of measurement points of 1600×1000 ; and image acquisition and data processing using MARK III software (FRT GmbH, München, Germany). Based on three-dimensional (3D) images, basic surface characteristics such as depth of the wear trace (S_a), roughness (R_a), and volume loss of analyzed materials were assessed.

3. Results and Discussion

3.1. Coefficient of Friction

The coefficient of friction (COF) as a function of the sliding distance for the tested materials is shown in Figure 7. In the case of the unreinforced matrix alloy (AlSi12), changes in the COF were unstable, with an average value of more than 0.4. As can be seen, the value of the COF during the entire sliding distance changed from $\mu = 0.35$ to $\mu = 0.5$. Such a high variation (equal to 0.15) is unacceptable. Such sudden changes in the COF are characteristic of AlSi alloys, but the obtained result provides a reference point for assessing the influence of reinforcing particles on the tribological properties of the tested composites.

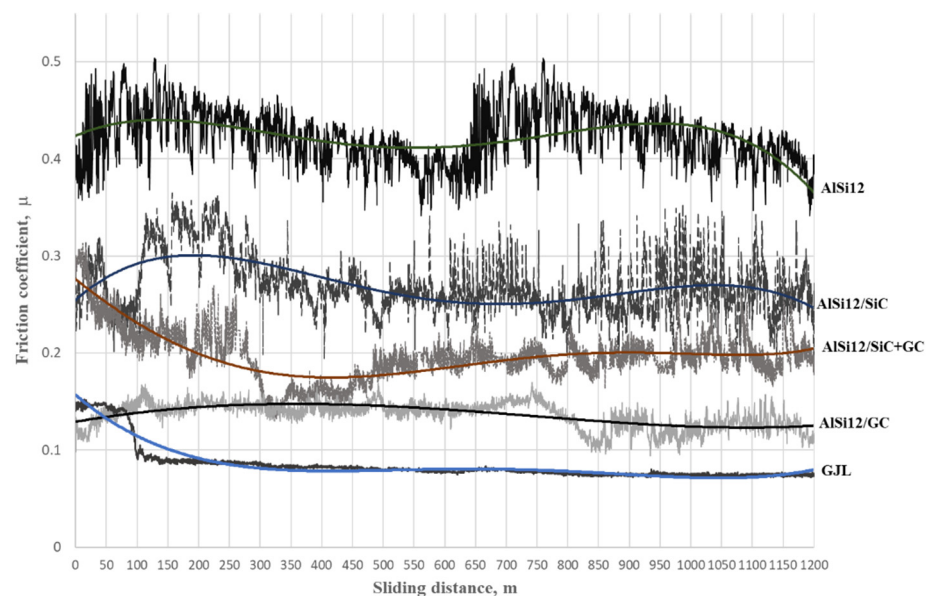


Figure 7. Friction coefficient (μ) versus sliding distance for the tested materials; the change of the trend for the tested materials was marked with continuous lines.

As can be seen, the changes in the COF were significantly different for the cast iron–cast iron tribological pair (Table 3). In this case, the value of the COF after a short run-in period (100 m) stabilized at $\mu = 0.07$ (Figure 7). Over the entire sliding distance, this value did not change, giving a very stable tribological cooperation.

Due to the use of silicon carbide as reinforcing particles (SiC_p), the effect of decreasing the value of the friction coefficient was obtained compared to the un-reinforced AlSi12 matrix alloy. However, in both cases, a similar unstable change in the COF was observed (Figure 7). During the sliding distance, the COF of the AlSi12/ SiC_p composite increased and decreased in the range of $\mu = 0.22$ to $\mu = 0.32$. In turn, the use of the hybrid reinforcement mixture ($\text{SiC}_p + \text{GC}_p$) decreased the COF ($\mu = 0.2$) and partially stabilized it, particularly after the brake-in period (500 m). The stabilization effect of the COF was significantly

visible in the case of the AlSi12/GC_p composite. As can be seen (black line in Figure 7), the COF of the AlSi12/GC_p was significantly lower than the other tested composites ($\mu = 0.12$). In the final stage of friction, the difference between the maximum and minimum values did not exceed 0.02 and was comparable to the values measured for iron materials.

3.2. Wear

The degree of surface wear under dry friction conditions was determined using the profilometry measurements. The volume loss of materials and the changes in surface geometry resulting from friction were evaluated. 3D images of the created wear tracks compared with the initial surfaces before friction of the materials are shown in Figures 8–12. The analysis of 3D images allowed for quantitative and qualitative assessments and an indication of the wear mechanism.

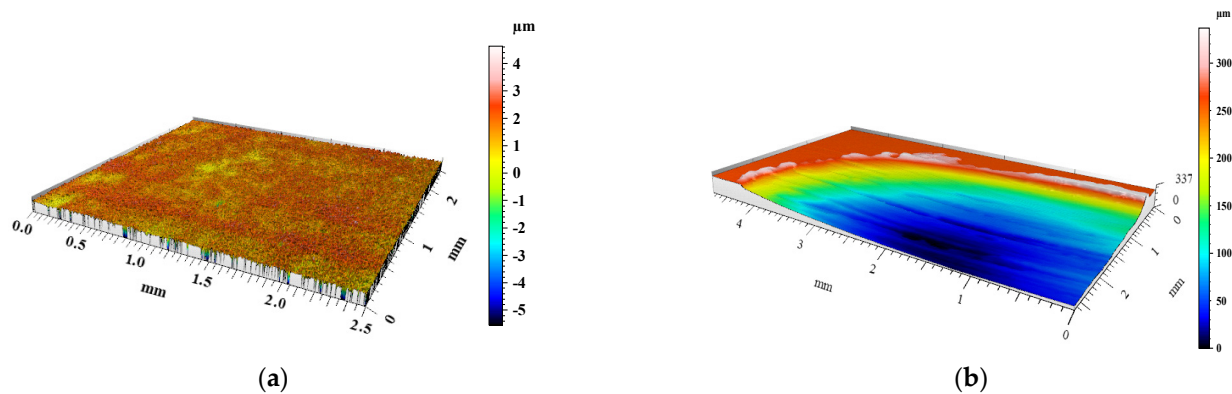


Figure 8. View of the AlSi12 matrix surface geometry: (a) before and (b) after dry friction test.

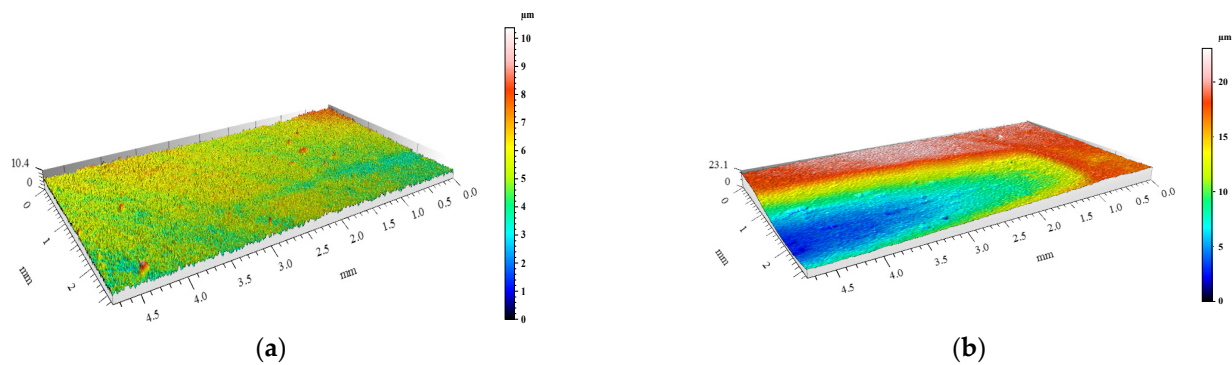


Figure 9. View of GJL cast-iron surface geometry: (a) before and (b) after dry friction test.

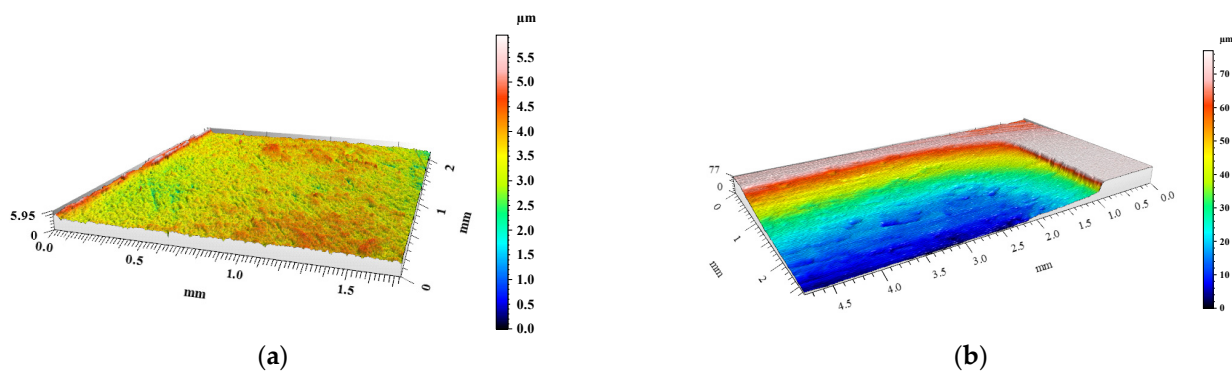


Figure 10. View of AlSi12/SiC_p composite surface geometry: (a) before and (b) after dry friction test.

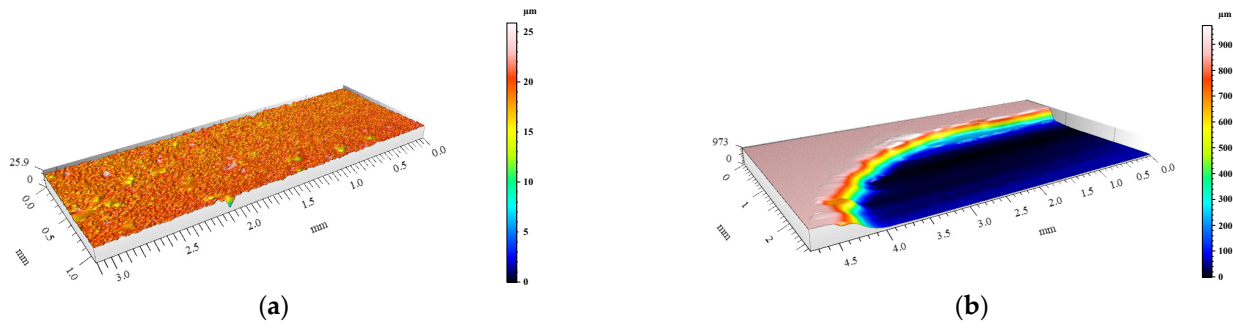


Figure 11. View of AISi12/GC_p composite surface geometry: (a) before and (b) after dry friction test.

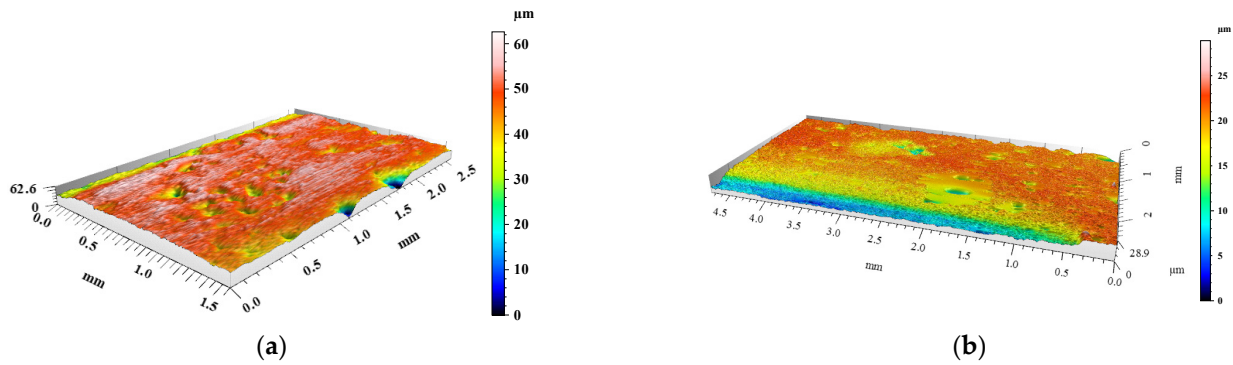


Figure 12. View of AISi12/SiC_p + GC_p hybrid composite surface geometry: (a) before and (b) after dry friction test.

Based on the 3D images (Figures 8–12), it can be concluded that all tested materials showed abrasive wear. However, there were significant differences in its intensity that can be compared due to the selected parameters. To evaluate the changes in surface geometry due to friction, the basic roughness parameters were used, including the arithmetical mean roughness value (*Ra*)—calculated as the arithmetical mean of the absolute values of the profile deviations from the mean line of the roughness profile, and (*Sa*)—arithmetical mean surface height (Figure 13), as well as the average depth of the wear trace (Figure 14).

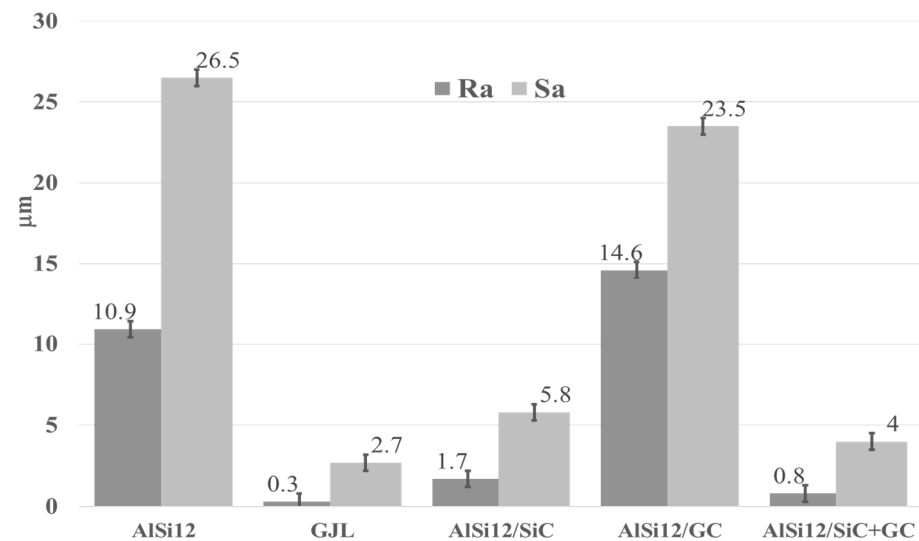


Figure 13. Roughness parameters value (*Ra*) and (*Sa*) of the wear track for all tested materials.

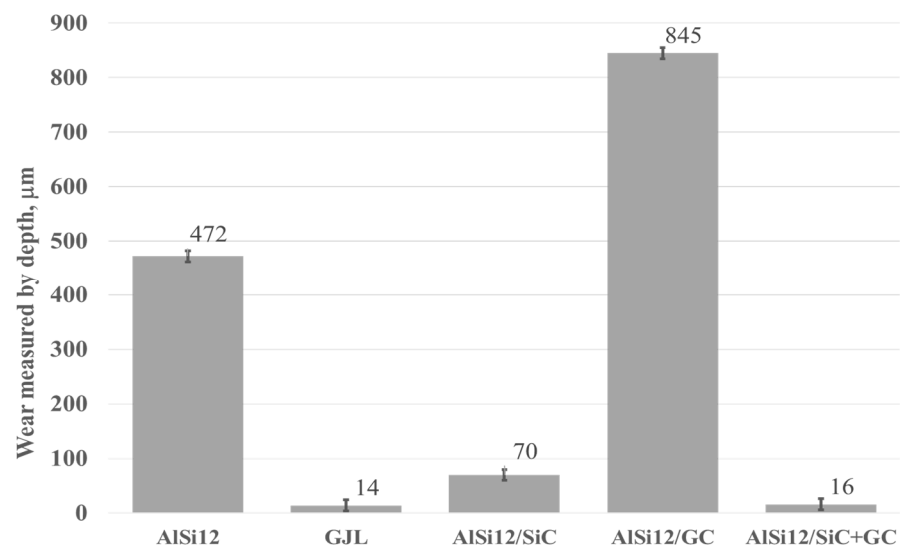


Figure 14. Depth of the wear track calculated based on 100 profiles.

Comparing the obtained images of the surface geometry after friction and the roughness parameters, it can be seen that the most intense wear occurred in the un-reinforced AISi12 matrix alloy (Figures 8 and 13) and in the composite reinforced with glassy carbon particles (Figures 11 and 13). In turn, the composite containing silicon carbide particles (Figures 10 and 13) and the composite with a hybrid mixture of SiC_p and GC_p (Figures 12 and 13) were characterized by significantly less abrasive wear.

Based on profilometry measurements and using our software capabilities, the volume loss of the materials was calculated. Then, the volume loss was used to compare the wear resistance of the tested materials. The results in the form of a graph are shown in Figure 15.

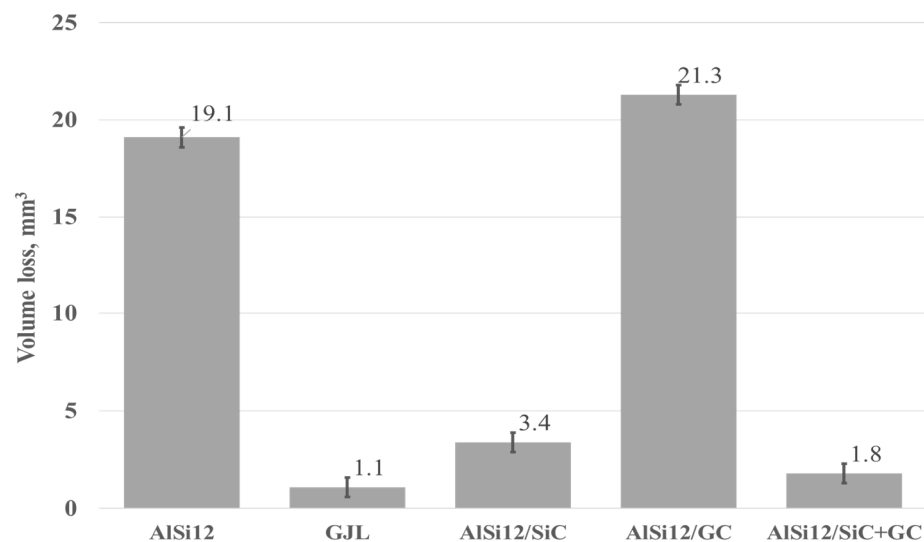


Figure 15. Volume loss of the tested materials calculated based on the wear track created under dry friction conditions.

As can be seen (Figure 15), the highest volume loss, and thus the lowest wear resistance under dry friction conditions, was recorded for the composite reinforced with glassy carbon particles (21.3 mm^3). Relatively high-volume losses also occurred for the un-reinforced AISi12 matrix alloy (19.1 mm^3). In turn, the lowest volume losses, and therefore the high resistance to abrasive wear, was noted for cast iron (1.1 mm^3). Whereas, among composite materials, the $\text{SiC}_p + \text{CG}_p$ hybrid reinforcement was the most advantageous (1.8 mm^3). In this case, the silicon carbide particles improved the abrasion resistance, while the addition

of glassy carbon played an important role as a lubricant for the cooperating surfaces. The SEM images of the wear tracks on the composites surface are shown in Figure 16.

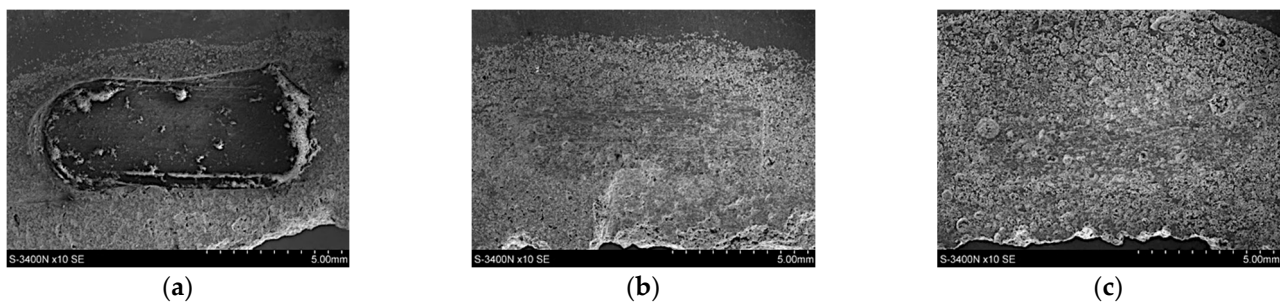


Figure 16. SEM images of the wear tracks on the composite surface: (a) AlSi12/GC_p; (b) AlSi12/SiC_p; and (c) AlSi12/SiC_p + GC_p hybrid composite: (a,b) LM; (c) SEM.

The obtained results can be related to the specific microstructure of the AlSi12/SiC_p + GC_p hybrid composite (Figure 17) and to the synergistic strengthening and self-lubricating effect. In this case, two parallel phenomena can be identified in the wear process. The first is the interaction of hard SiC_p particles with a cast-iron friction partner. As a result, SiC particles were periodically removed from the matrix alloy, which caused significant wear to the cast iron. The second phenomenon concerns the wear of GC_p particles, which were pulled from the matrix and crushed during the friction process, creating a solid sliding layer on the friction surface, which reduced the COF.

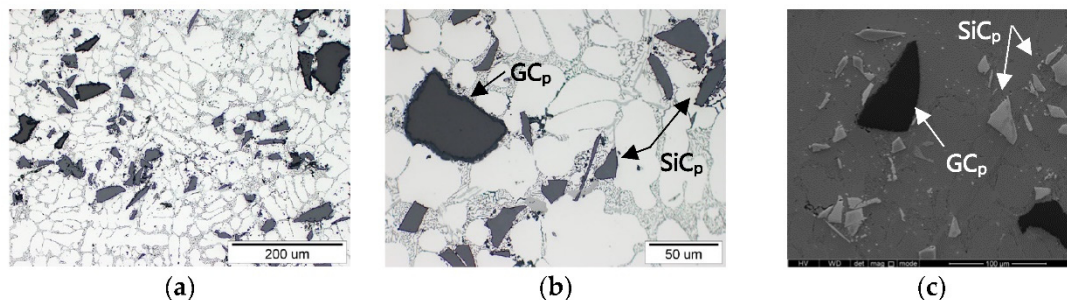


Figure 17. Microstructure of the AlSi12/SiC_p + GC_p hybrid composite: (a) and (b) LM; (c) SEM.

As can be seen (Figure 17), in the AlSi12/SiC_p + CG_p hybrid composite microstructure, larger glassy carbon particles were surrounded by much smaller SiC_p particles, which increased the hardness, provided load transfer through the surface, and wear resistance for the AlSi12 matrix alloy. In turn, the GC_p particles play an important role as a lubricant for both the working surfaces of the matrix and the SiC_p particles themselves. Similar results have been described by Myalski and Sleziona [42]. They found that the high hardness of glassy carbon particles (comparable to SiC particles) did not cause major damage to the cast iron pin that served as the friction partner to the composite material. The authors explained these results by the fact that mainly glassy carbon particles with a low COF participated in the friction process. Furthermore, in our previous research [13,28], it was shown that the presence of glassy carbon, both in the form of particles and spheres in various types of Al/SiC_p composites, not only decreased and stabilized the COF but also reduced the wear of the friction partner in tribological couples.

In turn, the presented results confirmed that the presence of single glassy carbon particles inside the aluminum matrix alloy (AlSi12/GC_p composite, Figure 18) has a much lower effect on the wear resistance. However, it helped reduce and stabilize the COF.

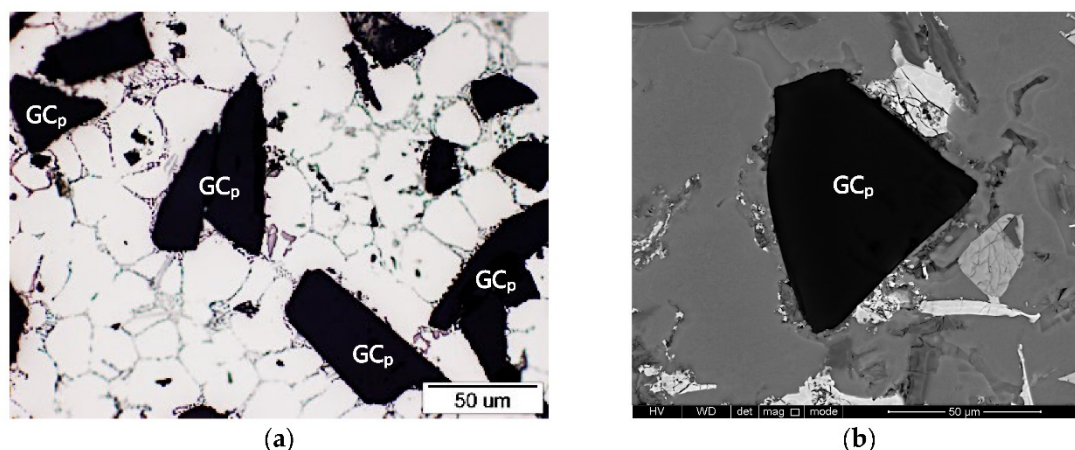


Figure 18. Microstructure of AlSi12/GC_p composite: (a) LM; (b) SEM.

4. Conclusions

The conducted tribological investigation under dry friction conditions allowed for an evaluation of the behavior of materials in extremely unfavorable working conditions.

The obtained results and their analysis clearly indicate that the highest COF was recorded for the un-reinforced matrix, and the average value was $\mu = 0.42$. In this case, a high-volume loss of the material was also observed, at the level of 19 mm^3 . It was shown that introducing reinforcement particles into the AlSi12 matrix alloy significantly changed the friction conditions. However, the glassy carbon particles (GC_p) decreased the COF (average $\mu = 0.12$) but did not increase the wear resistance of the material. In this case, the volume loss and depth of the friction trace were the highest among all tested materials (21.3 mm^3 and 0.85 mm , respectively). In turn, the SiC_p reinforcement decreased the COF to $\mu = 0.26$ and also significantly reduced the material wear. The wear depth was almost seven times smaller than that of the un-reinforced matrix alloy. The material that gave the most beneficial effect, a low COF ($\mu = 0.18$), and increased the wear resistance (a volume loss of 1.8 mm^3) was the use of a hybrid reinforcement (SiC_p + GC_p).

The results described here demonstrate that AlSi12/SiC_p and AlSi12/SiC_p + GC_p composites showed significantly better tribological properties than the commercial AlSi12CuNiMg alloy and could be applied to a P-R-C assembly. The results also provide an introduction to further research related to the development of new materials and technological concepts aimed at shaping a local AlSi/SiC_p insert in the groove of the top compression rings intended for compression ignition engine pistons.

Author Contributions: Conceptualization, A.J.D., J.W. and M.D.; methodology, A.J.D. and J.W.; software, J.W.; formal analysis, A.J.D. and J.W.; investigation, A.J.D., J.W., M.D. and M.S.; writing—original draft preparation, A.J.D., J.W., M.S.; writing—review and editing, A.J.D.; visualization, A.J.D., J.W., M.S.; supervision, A.J.D.; project administration, A.J.D.; funding acquisition, A.J.D. and M.D. All authors have read and agreed to the published version of the manuscript.

Funding: This research was co-funded by the National Centre for Research and Development, Poland, grant number TANGO2/340272/NCBR/2017, “Development of technology for manufacturing of composite insert to the local reinforcement of aluminum castings” and by the Silesian University of Technology from subsidies for statutory activities, project no. 11/030/BK_22/1082.

Institutional Review Board Statement: Not applicable.

Informed Consent Statement: Not applicable.

Data Availability Statement: Not applicable.

Conflicts of Interest: The authors declare no conflict of interest. The funders had no role in the design of the study; in the collection, analyses, or interpretation of data; in the writing of the manuscript; or in the decision to publish the results.

References

1. Trapy, J.D.; Damiral, P. An Investigation of Lubricating System Warm-up for the Improvement of Cold Start Efficiency and Emissions of S.I. Automotive Engines. *SAE Trans.* **1990**, *99*, 1635–1645.
2. Dziubak, T.; Dziubak, S.D. A Study on the Effect of Inlet Air Pollution on the Engine Component Wear and Operation. *Energies* **2022**, *15*, 1182. [[CrossRef](#)]
3. Suchecki, J. Reducing mechanical losses of the engine as a method of reducing CO₂. *Combust. Engines* **2013**, *154*, 496–499.
4. Rohatgi, P.K.; Gupta, N.; Daoud, A. Synthesis and processing of cast metal matrix composites and their applications. *ASM Handb.* **2008**, *15*, 1149–1164.
5. Bieniaś, J.; Walczak, M.; Surowska, B.; Sobczak, J. Microstructure and corrosion behavior of aluminium fly ash composites. *J. Optoelektron. Adv. Mater.* **2003**, *5*, 493–502.
6. Degischer, H.P.; Prader, P.; Marchi, C.S. “Assessment of Metal Matrix Composites for Innovations”—Intermediate report of a European Thematic Network. *Compos. Part A Appl. Sci. Manuf.* **2001**, *32*, 1161–1166. [[CrossRef](#)]
7. Macke, A.; Schultz, B.F.; Rohatgi, P. Metal Matrix Composites offer the Automotive Industry an Opportunity to Reduce Vehicle Weight, Improve Performance. *Adv. Mater. Proc.* **2012**, *170*, 12–23.
8. Sobczak, J.; Wojciechowski, S. The current trends in the practical application of metal matrix composites. *Kompozyty (Composites)* **2002**, *2*, 24–37.
9. Kurtyka, P.; Rylko, N.; Tokarski, T.; Wójcicka, A.; Pietras, A. Cast aluminium matrix composites modified with using FSP process—Changing of the structure and mechanical properties. *Compos. Struct.* **2015**, *133*, 959–967. [[CrossRef](#)]
10. Przystacki, D.; Szymański, P.; Wojciechowski, S. Formation of surface layer in metal matrix composite A359/20SiCP during laser assisted turning. *Compos. Part A Appl. Sci. Manuf.* **2016**, *91*, 370–379. [[CrossRef](#)]
11. Posmyk, A.; Malski, J. Designing cylinder liners made from hybrid composites containing solid lubricants. *Compos. Theory Pract.* **2016**, *16*, 15–19.
12. Posmyk, A.; Filipczyk, J. Aspects of the applications of composite materials in combustion engines. *J. KONES Powertrain Transp.* **2013**, *20*, 357–361. [[CrossRef](#)]
13. Dolata, A.J.; Dyzia, M.; Jaworska, L.; Putyra, P. Cast hybrid composites designated for air compressor pistons. *Arch. Metall. Mater.* **2016**, *61*, 705–708. [[CrossRef](#)]
14. Manasijevic, S.; Radisa, R.; Markovic, S.; Acimovic-Pavlovic, Z.; Raic, K. Thermal analysis and microscopic characterization of the piston alloy AlSi13Cu4Ni2Mg. *Intermetallics* **2011**, *19*, 486–492. [[CrossRef](#)]
15. Abouei, V.; Saghafian, H.; Shabestari, S.G.; Zarghami, M. Effect of Fe-rich intermetallics on the wear behavior of eutectic Al–Si piston alloy (LM13). *Mater. Des.* **2010**, *31*, 3518–3524. [[CrossRef](#)]
16. Orłowicz, A.W.; Tupaj, M.; Mróz, M.; Trytek, A. Combustion Engine Cylinder Liners Made of Al–Si Alloys. *Arch. Foundry Eng.* **2015**, *15*, 71–74. [[CrossRef](#)]
17. Yanga, Y.; Li, Y.; Wua, W.; Zhao, D.; Liu, X. Effect of existing form of alloying elements on the microhardness of Al–Si–Cu–Ni–Mg piston alloy. *Mater. Sci. Eng. A* **2011**, *528*, 5723–5728. [[CrossRef](#)]
18. Huang, X.; Liu, C.; Lv, X.; Liu, G.; Li, F. Aluminum alloy pistons reinforced with SiC fabricated by centrifugal casting. *J. Mater. Process. Technol.* **2011**, *211*, 1540–1546. [[CrossRef](#)]
19. Soltani, S.; Khosroshahi, R.A.; Mousavian, R.T.; Jiang, Z.; Boostani, A.F.; Brabazon, D. Stir casting process for manufacture of Al–SiC composites. *Rare Met.* **2015**, *36*, 581–590. [[CrossRef](#)]
20. Kumar, R.; Bhowmick, H.; Gupta, D. Progress on the development of aluminium metal matrix composite as an alternative piston material—A review. *J. Emerg. Technol. Innov. Res.* **2019**, *6*, 414–419.
21. Kaur, K.; Anant, R.; Pandey, O.P. Tribological behaviour of SiC particle reinforced Al–Si alloy. *Tribol. Lett.* **2011**, *44*, 41–58. [[CrossRef](#)]
22. Arsha, A.G.; Jayakumar, E.; Rajan, T.P.; Antony, V.; Pai, B.C. Design and fabrication of functionally graded in-situ aluminium composites for automotive pistons. *Mater. Des.* **2015**, *88*, 1201–1209. [[CrossRef](#)]
23. Venkatarreddy, K.; Chandrashekar Goud, V. Design and analysis of the piston by using composite materials. *Int. J. Prof. Eng. Stud.* **2016**, *7*, 153–162.
24. Vencl, A.; Rac, A.; Bobic, I. Tribological Behaviour of Al-Based MMCs and their Application in Automotive Industry. *Trib. Ind.* **2004**, *26*, 31–38.
25. Prasad, S.; Asthana, R. Aluminum Metal–Matrix Composites for Automotive Applications: Tribological Considerations. *Tribol. Lett.* **2004**, *17*, 445–453. [[CrossRef](#)]
26. Nam, T.H.; Requena, G.; Degischer, P. Thermal expansion behaviour of aluminum matrix composites with densely packed SiC particles. *Compos. Part A: Appl. Sci. Manuf.* **2008**, *39*, 856–865. [[CrossRef](#)]
27. Dyzia, M. Aluminum Matrix Composite (AlSi7Mg2Sr0.03/SiCp) Pistons Obtained by Mechanical Mixing Method. *Materials* **2017**, *11*, 42. [[CrossRef](#)]
28. Dolata, A.J.; Dyzia, M.; Wiczorek, J. Tribological Properties of Single (AlSi7/SiCp, AlSi7/GCsf) and Hybrid (AlSi7/SiCp + GCsf) Composite Layers Formed in Sleeves via Centrifugal Casting. *Materials* **2019**, *12*, 2803. [[CrossRef](#)]
29. Niewczas, A.; Koszałka, G.; Guzik, M. Modeling of collaboration between the piston ring and the piston groove shelf in an internal combustion engine. *Eksplot. I Niezawodn. Maint. Reliab.* **2006**, *4*, 82–86.

30. Wolff, A.; Piechna, J. Numerical simulation of piston ring pack operation with regard to ring twist effects. *Arch. Mech. Eng.* **2007**, *LIV*, 65–99. [[CrossRef](#)]
31. Wolff, A. Experimental verification of the model of piston ring pack operation of an internal combustion engine. *Arch. Mech. Eng.* **2009**, *LVI*, 73–90.
32. Wolff, A. Numerical analysis of piston ring pack operation. *Combust. Engines* **2009**, *137*, 128–141. [[CrossRef](#)]
33. Forero, J.D.; Ochoa, G.V.; Rojas, J.P. Effect of the Geometric Profile of Top Ring on the Tribological Characteristics of a Low-Displacement Diesel Engine. *Lubricants* **2020**, *8*, 83. [[CrossRef](#)]
34. Selmani, E.; Delprete, C.; Bisha, A. Cylinder liner deformation orders and efficiency of a piston ring- pack. In Proceedings of the ICPEME, E3S Web of Conferences, Prague, Czech Republic, 16–19 February 2019; Volume 95, p. 04001. [[CrossRef](#)]
35. Piątkowski, J.; Czerepak, M. The Crystallization of the AlSi9 Alloy Designed for the Alfin Processing of Ring Supports in Engine Pistons. *Arch. Foundry Eng.* **2020**, *2*, 65–70. [[CrossRef](#)]
36. Manasijević, S.; Radiša, R.; Brodarac, Z.Z.; Dolić, N.; Djurdjevic, M. Al-Fin bond in aluminum piston alloy & austenitic cast iron insert. *Int. J. Met.* **2015**, *9*, 27–32.
37. Diesel Engine Piston. Available online: <https://zloteczki.pl/oferta/tloki/?lang=en> (accessed on 12 April 2022).
38. Dolata-Grosz, A. Interaction of Al-Si alloys with SiC/C ceramic particles and their influence on microstructure of composites. *Solid State Phenom.* **2011**, *176*, 55–62. [[CrossRef](#)]
39. Dolata, A.J.; Dyzia, M. Aspects of fabrication aluminium matrix heterophase composites by suspension method. *IOP Conf. Ser. Mater. Sci. Eng.* **2012**, *35*, 012020. [[CrossRef](#)]
40. Dolata, A.J.; Mróz, M.; Dyzia, M.; Jacek-Burek, M. Scratch testing of AlSi12/SiCp composite layer with high share of reinforcing phase formed in the centrifugal casting process. *Materials* **2020**, *13*, 1685. [[CrossRef](#)]
41. Dolata, A.J.; Golak, S.; Ciepłiński, P. The eulerian multiphase model of centrifugal casting process of particle reinforced Al matrix composites. *Compos. Theory Pract.* **2017**, *17*, 200–205.
42. Myalski, J.; Ślezionek, J. Glassy carbon particles as component to modification of tribological properties. *J. Mater. Processing Technol.* **2006**, *175*, 291–298. [[CrossRef](#)]